Available online at www.sciencedirect.com
SCIENCE DIRECT®
Polyhedron 24 (2005) 807–821
POLYHEDRON
www.elsevier.com/locate/poly

Complexes derived from hydrolytically 'unstable' hydrazone ligands – Some unexpected products

Timothy L. Kelly [a], Victoria A. Milway [a], Hilde Grove [a], Virginie Niel [a], Tareque S.M. Abedin [a], Laurence K. Thompson [a,*], Liang Zhao [a], Rosemary G. Harvey [a], David O. Miller [a], Michael Leech [b], Andrés E. Goeta [b], Judith A.K. Howard [b]

[a] *Department of Chemistry, Memorial University, Elizabeth Avenue, St. John's, Nfld, Canada A1B 3X7*
[b] *Department of Chemistry, University of Durham, Durham DH1 3LE, UK*

Received 15 October 2004; accepted 11 February 2005
Available online 13 April 2005

Abstract

Polyfunctional ligands derived from condensation reactions in which small molecules, e.g., water, an alcohol, etc., are eliminated can suffer the ravages of hydrolytic attack on reaction with transition metal ions in aqueous based solvents, or solvents containing small amounts of water. A series of such reactions is described involving hydrazone based ligands, in which hydrolyzed ligand fragments, and their resulting coordination complexes, are produced. Structures are reported to identify these products, which reveal some unexpected ligand rearrangements. Variable temperature magnetic data are discussed for some dinuclear complexes, and a DFT study is presented to rationalize an unusual ligand transformation.

Keywords: Hydrazone ligands; Complexes; Copper; Nickel; Iron; Cobalt; Hydrolysis; Structure; Magnetism

1. Introduction

Ligands derived from condensation reactions, which involve elimination of small molecules, e.g., water, or an alcohol, are at risk of hydrolytic attack in solvents that contain water, when reacted with transition metal salts. Such reactions can be promoted or catalyzed by the presence of the transition metal ion, whose high ionic potential can in many cases exert a significant polarizing effect on the hydrolytically vulnerable bonds. In some cases the complexes which are formed contain 'expected' hydrolysis products, but in other cases some surprising results can occur.

In a recent report the ligand L1 was shown to be hydrolytically unstable in the presence of $CuBr_2$ in aqueous acetonitrile, and a mixed oxidation state $Cu(II)_4Cu(I)_2$ complex of the ligand picolinamide hydrazone (PAH) was produced (Scheme 1) [1]. The reduction of copper(II) was associated with the presence of acetonitrile and the reducing capacity of salicylaldehyde, detected during the reaction. The symmetrical open chain diazine ligands PAHAP and PZHPZ (Chart 1) react with Fe(III) nitrate in aqueous solution to spontaneously form the reduced dinuclear $[Fe(II)_2(L)_3]^{4+}$ (L = PAHAP, PZHPZ) complex ions in low yield, suggesting the formation of hydrazine based fragments, presumably resulting from hydrolysis of an imine group, which act as metal ion reductants. In the case of PAHAP, reaction with Fe(III) nitrate also produces the complex ion $[Fe(III)(POAP-H)(H_2O)_2(NO_3)]^{2+}$ (POAP, Chart 1) as a minor product, indicating the imine group as an initial point of hydrolytic

* Corresponding author. Tel.: +1 709 737 8750; fax: +1 709 737 3702.
E-mail address: lthomp@mun.ca (L.K. Thompson).

0277-5387/$ - see front matter © 2005 Elsevier Ltd. All rights reserved.
doi:10.1016/j.poly.2005.02.016

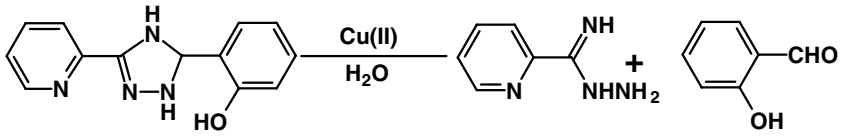

L1 PAH

Scheme 1.

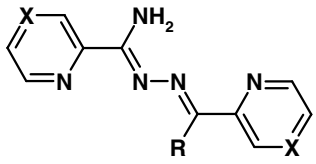

PAHAP (X=CH, R=NH_2), PZHPZ (X=N, R=NH_2), POAP (X=CH, R=OH)

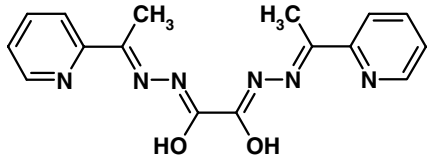

L2

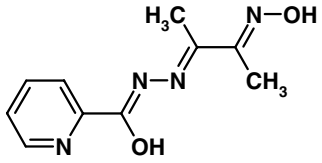

L3

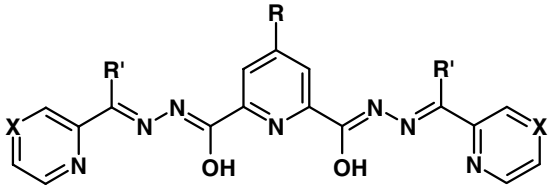

L4 (R=Cl, R'=Phenyl, X=CH)
L5 (R=Cl, R'=NH_2, X=N)

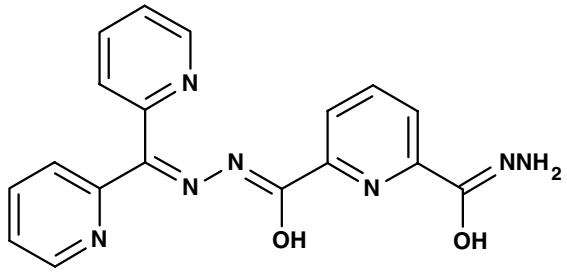

L6

Chart 1.

attack in the formation of the analogous acyl ligand, presumably promoted by the coordination of the highly polarizing Fe(III) center [2].

The present report discusses transition metal complexes derived from a group of extended polyfunctional diazine ligands L2–L6 (Chart 1), in which metal ion based ligand hydrolysis has occurred at a 'vulnerable' ligand C=N site, with the formation of complexes containing rearranged ligands and ligand fragments. The ligand L3 has been reported elsewhere, along with a number of coordination complexes, but there is no evidence for ligand hydrolysis [3]. The ligand L4 undergoes hydrolysis in the presence of Co(II) in air, and with Cu(II) salts, but remains intact on reaction with Ni(II) carbonate. Structures are reported for some iron, nickel and copper complexes, and the magnetic properties of some polynuclear copper and iron products are discussed. DFT studies are highlighted in one nickel case where an unusual ligand transformation takes place.

2. Experimental

2.1. Physical measurements

Infrared spectra were recorded as Nujol mulls using a Mattson Polaris FTIR instrument. Mass spectra were obtained using a VG Micromass 7070HS spectrometer and an Agilent 1100 series LC/MSD spectrometer. C, H, N analyses on dried samples were carried out by the Canadian Microanalytical Service, Delta, B.C., Canada. Variable temperature magnetic data (2–300 K) were obtained with a Quantum Design MPMS5S Squid magnetometer operating at 0.1–5.0 T. Calibrations were carried out with a palladium standard cylinder, and the normal diamagnetic corrections were applied.

2.2. Syntheses

2.2.1. L2

2-Acetyl pyridine (3.70 g, 0.0300 mol) was dissolved in methanol (100 mL). Oxalic acid dihydrazide (1.77 g, 0.0150 mol) was added and the mixture refluxed for 12 h. A white precipitate formed, which was separated by filtration, washed with methanol and ether and dried under vacuum (Yield 4.4 g, 91%); m.p. dec. >260 °C. Mass spectrum (*m*/*z*) 189, 162, 134, 106, 78 (molecular ion not observed). IR (ν cm^{-1}) 1681 (C=O), 1012 (pyr). *Anal*. Calc. for $C_{16}H_{16}N_6O_2$: C, 59.25; H, 4.97; N, 25.91. Found: C, 58.67; H, 4.94; N, 25.72%.

2.2.2. L3

Butanedione monoxime (5.04 g, 0.0498 mol) was dissolved in absolute ethanol (40 mL). Picolinic acid hydrazide (3.32 g, 0.0242 mol) was added and the mixture refluxed for several hours with the formation of a white suspended solid. The fine white precipitate was filtered off and washed with methanol (Yield 4.86 g, 91%). Recrystallization from acetonitrile produced colorless crystals, but crystals suitable for structural determination were obtained from the reaction of $Gd(NO_3)_3$ and L3 in a MeCN, MeOH, H_2O mixture, in which there appeared to be no Gd complex formation. Mass spectrum (*m*/*z*) 221 (MH^+), 203, 182, 124, 108, 79. IR (ν cm^{-1}) 3343 (OH), 1677 (C=O), 995 (pyr). *Anal*. Calc. for $C_{10}H_{12}N_4O_2$: C, 54.55; H, 5.45; N, 25.45. Found: C, 54.55; H, 5.58; N, 25.41%.

2.2.3. L4

2-Benzoylpyridine (7.44 g, 41 mmol) was dissolved in $CHCl_3$ (220 mL). 4-Chloro-2,6-pyridine carboxylic acid hydrazide (2.30 g, 10 mmol) was added, along with dry methanol (30 mL), and the mixture was refluxed for 72 h. The volume of the resulting solution was reduced by about 50%, and methanol (30 mL) was added and heating continued until a white precipitate formed. The precipitate was collected by suction filtration, and washed with methanol and diethyl ether (Yield 3.6 g, 65%); m.p. 288–294 °C. Mass spectrum (*m*/*z*) 560 (M), 542 ($M - H_2O$). IR (ν, cm^{-1}) 1697 (C=O), 1574 (C=N), 997 (py). *Anal*. Calc. for $C_{31}H_{22}N_7O_2Cl\cdot 0.5H_2O$: C, 65.49; H, 4.05; N, 17.25. Found: C, 65.25; H, 3.95; N, 17.33%.

2.2.4. L6

2,6-Pyridine carboxylic acid hydrazide (0.93 g, 5.0 mmol) was added to a solution of dipyridyl ketone (1.84 g, 10 mmol) in absolute ethanol (50 mL), and the mixture was refluxed for 10 h. The product formed as a white solid during the reaction, and was filtered off, washed with ethanol and dried in air (Yield 1.7 g, 90%). *Anal*. Calc. for $C_{18}H_{15}N_7O_2(C_{29}H_{21}N_9O_2)_{0.22}$; C, 61.34; H, 4.14; N, 26.35. Found: C, 61.31; H, 4.09; N, 26.19%. The reaction appears to have produced a mixture of mono and disubstituted ligands, with about 20% disubstituted. Separation could not be effected cleanly, and so the mixture was used in the reaction with $Cu(NO_3)_2$ (vide infra).

*2.2.5. $[Cu_2(L7)_2(C_2O_4)(H_2O)_2(NO_3)_2]$ (**1**), $[Cu_2(L7)_2(C_2O_4)](ClO_4)_2$ (**2**)*

L2 (0.324 g, 1.00 mmol) was added to a warm solution of $Cu(NO_3)_2\cdot 3H_2O$ (0.483 g, 2.00 mmol) in $MeOH/H_2O$ (10/5 mL), forming a green solution. Dark green crystals, suitable for a structural analysis, were obtained on standing the solution at room temperature over several days (Yield 0.37 g, 45%). *Anal*. Calc. for $[(C_7H_9N_3)_2Cu_2(C_2O_4)(H_2O)_2(NO_3)_2]$: C, 29.78; H, 3.44; N, 17.36. Found: C, 29.79; H, 3.33; N, 17.67%. **2** was produced under similar conditions using copper(II) perchlorate (Yield 50%). *Anal*. Calc. for $[(C_7H_9N_3)_2Cu_2(C_2O_4)](ClO_4)_2$: C, 28.08; H, 2.65; N, 12.28. Found: C, 28.37; H, 2.63; N, 12.24%.

*2.2.6. $[Ni(L8)]Br\cdot CHCl_3$ (**3**)*

$NiBr_2$ (0.24 g, 1.0 mmol) was suspended in 50/50 $CH_3CN/MeOH$ (20 mL). L3 (0.20 g, 0.90 mmol) was added and the mixture was heated with stirring. A clear orange solution formed, which was filtered and allowed to stand, forming a red orange powder (Yield 55%). Recrystallization from $CHCl_3$ gave red block shaped crystals suitable for structural determination. A similar reaction with $Ni(ClO_4)_2\cdot 6H_2O$ and $Ni(NO_3)_2\cdot 6H_2O$ gave $[Ni(L8)](ClO_4)\cdot H_2O$ and $[Ni(L8)](NO_3)\cdot 2H_2O$, respectively, as red powders (Yield 60–70%). *Anal*. Calc. for $[(C_{16}H_{15}N_6O_2)Ni](ClO_4)\cdot H_2O$: C, 38.55; H, 3.41; N, 16.86. Found: C, 38.27; H, 3.30; N, 16.73%. *Anal*. Calc. for $[(C_{16}H_{15}N_6O_2)Ni](NO_3)\cdot 2H_2O$: C, 40.08; H, 3.97; N, 20.46. Found: C, 39.56; H, 3.29; N, 20.37%. Similar infrared spectral bands associated with the ligand L8 are observed in all three compounds.

*2.2.7. $[Cu_2(L9)(L10)]\cdot 2H_2O\cdot CH_3OH\cdot L11$ (**4**)*

L4 (0.10 g, 0.18 mmol) was added to a solution of copper acetate (0.18 g, 0.45 mmol) in methanol (20 mL), forming a clear brown solution. Red brown crystals of **4**, suitable for a structural determination, were obtained in low yield (35 mg) after allowing the solution to evaporate to a small volume. *Anal*. Calc. for $[(C_{19}H_{11}N_4O_3Cl)(C_7H_2NO_4Cl)Cu_2](C_{12}H_9N_3)\cdot 7H_2O$: C, 44.53; H, 3.52; N, 10.94. Found: C, 44.47; H, 2.67; N, 11.08%. The dried analytical sample contains no methanol.

*2.2.8. $[Fe_2(PZHPZ)_3](ClO_4)_4\cdot 2CH_3CN$ (**5**)*

L5 [4] (0.070 g, 0.16 mmol) was added to a degassed solution of $Fe(ClO_4)_2\cdot 6H_2O$ (0.122 g, 0.48 mmol) in CH_3CN (10 mL) under an Ar atmosphere. The mixture was heated to reflux for 10 min., and then left at room temperature. Purple crystals formed after several days in the Ar atmosphere (Yield 50 mg), which were kept under the mother liquor prior to structural analysis. Solvent loss occurred on exposure of the bulk sample to air. *Anal*. Calc. for $[(C_{10}H_{10}N_8)_3Fe_2](ClO_4)_4\cdot 7H_2O$: C, 26.45; H, 3.26; N, 24.68. Found: C, 26.40; H, 2.69; N, 24.93% (air dried sample).

*2.2.9. $[Cu_2(L12\text{-}2H)](NO_3)_2\cdot 1.5H_2O$ (**6**)*

L6 (0.25 g, 0.50 mmol) was added to a solution of $Cu(NO_3)_2\cdot 3H_2O$ (0.72 g, 3.0 mmol) in $MeOH/H_2O$ (20/10 mL) and the mixture was warmed. Green crystals were obtained from the resulting green solution on standing at room temperature (Yield 0.21 g, 68%). *Anal*.

Calc. for $(C_{18}H_{11}N_5O_3)Cu_2(NO_3)_2\cdot 1.5H_2O$. C, 34.68; H, 2.26; N, 15.73. Found: C, 34.50; H, 2.12; N, 16.10%.

2.2.10. [Ni(L4-2H)] (7)

$NiCO_3$ (0.18 g, 1.5 mmol) was suspended in 1:1 MeCN/EtOH (20 mL). L4 (0.10 g, 018 mmol) was added and the mixture was heated. Water (5 mL) was added and heating continued for 15 min. with the formation of a red solution. The solution was filtered to remove excess nickel carbonate, and allowed to stand at room temperature. Red crystals suitable for structural analysis formed after two days (Yield 60 mg, 55%).

2.3. X-ray crystallography

The diffraction intensities of a green prismatic crystal of **1** were collected with graphite-monochromatized Mo Kα X-radiation (rotating anode generator) using a Bruker P4/CCD diffractometer at 193(1) K to a maximum 2θ value of 52.8°. The data were corrected for Lorentz and polarization effects. The structure was solved by direct methods [5,6]. All atoms except hydrogen atoms were refined anisotropically. Hydrogen atoms were placed in calculated positions with isotropic thermal parameters set to 20% greater than their bonded partners, and were not refined. Neutral atom scattering factors [7] and anomalous-dispersion terms [8,9] were taken from the usual sources. All other calculations were performed with the teXsan [10] crystallographic software package.

Diffraction data were collected for **3**–**5** in a similar manner. Abbreviated structural data for **1**, **3**–**5** are reported in Table 1.

The diffraction intensities of a colourless single crystal of L3 were collected with graphite-monochromated Cu Kα X-radiation using a Rigaku AFC6S diffractometer at 299(1) K and the ω–2θ scan technique to a 2θ value of 120.1°. The data were corrected for Lorentz and polarization effects. The structure was solved by direct methods [5,6]. All atoms except hydrogen atoms were refined anisotropically. Hydrogen atoms were introduced with isotropic thermal parameters set 20% greater than those of their bonded partners at the time of their inclusion. They were optimized by positional refinement. Neutral atom scattering factors [7] and anomalous-dispersion terms [8,9] were taken from the usual sources. All calculations were performed with the teXsan [10] crystallographic software package. Diffraction data for **7** (red prism) were collected in a similar manner. Abbreviated structural details for L3 and **7** are listed in Table 1.

Diffraction data for a single crystal of **6** (green prism, $0.30\times0.40\times0.20$ mm) were collected using a Bruker SMART CCD diffractometer, equipped with an Oxford Cryostream N_2 cooling device [11], with graphite monochromatized Mo Kα radiation. Cell parameters were determined and refined using the SMART software [12a], raw frame data were integrated using the SAINT program [12b] and the structure was solved using direct methods and refined by full-matrix least squares on F^2 using SHELXTL [13]. Non-hydrogen atoms were refined with anisotropic atomic displacement parameters (adps). Hydrogen atoms bound to carbon atoms were placed in geometrically calculated positions with isotropic adps 1.2 times that of the parent atom.

Table 1
Summary of crystallographic data for **1**, L3, **3**–**7**

Compound	**1**	L3	**3**	**4**	**5**	**6**	**7**
Empirical formula	$C_{32}H_{44}N_{16}Cu_4O_{24}$	$C_{10}H_{12}O_2N_4$	$C_{34}H_{32}Br_2Cl_6N_{12}Ni_2O_4$	$C_{39}H_{30}N_8O_{10}Cl_2Cu_2$	$C_{34}H_{36}N_{26}O_{16}Cl_4Fe_2$	$C_{18}H_{19}N_7O_{13}Cu_2$	$C_{31}H_{20}N_7O_2NiCl$
Formula weight	1286.96	220.23	1162.66	968.69	1318.39	668.48	616.7
Wavelength (Å)	0.71073	1.54178	0.71073	0.71073	0.71073	0.71073	0.71703
Crystal system	triclinic	monoclinic	triclinic	monoclinic	monoclinic	monoclinic	monoclinic
Space group	$P\bar{1}$	$P2_1/c$ (#14)	$P\bar{1}$ (#2)	$C2/c$	$C2/c$ (#15)	Cc	Cc
a (Å)	10.1578(8)	5.706(4)	7.3323(11)	29.927(3)	17.4322(13)	25.513(2)	14.405(3)
b (Å)	13.4753(11)	25.812(4)	11.5251(16)	8.8728(8)	15.6919(12)	7.1249(6)	17.663(5)
c (Å)	17.8890(14)	7.337(3)	13.7813(19)	30.906(3)	20.7481(15)	16.8915(14)	10.689(4)
α (°)	103.473(1)	90	71.791(3)	90	90	90	90
β (°)	90.963(1)	100.19(4)	75.089(3)	109.832(2)	99.335(2)	129.9970(10)	103.73(3)
γ (°)	105.493(2)	90	79.892(3)	90	90	90	90
V (Å^3)	2286.5(3)	1063.6(7)	1063.3(2)	7720.1(12)	5600.4(6)	2352.2(3)	2642(1)
$D_{calc.}$ (g cm^{-3})	1.869	1.375	30821.816	1.667	1.563	1.888	1.550
Temperature (K)	193(2)	299(1)	193(2)	193(2)	193(2)	100(2)	299(1)
Z	2	4	1	8	4	4	4
μ (cm^{-1})	19.42	8.31	32.01	13.12	7.94	1.894	8.81
Reflections/parameters	8631/704	977/182	3698/280	7878/550	5733/404	5371/437	2206/376
Final R_1, wR_2	0.0645, 0.200	0.056, 0.057 (R,R_w)	0.0562, 0.1385	0.0443, 0.1114	0.064, 0.2049	0.0171, 0.0465	0.043, 0.040 (R,R_w)

$R_1 = \sum[||F_o| - |F_c||]/\sum|F_o|$, $wR_2 = [\sum[w(|F_o|^2 - |F_c|^2)^2]/\sum[w(|F_o|^2)^2]]^{1/2}$.
$R = \sum||F_o| - |F_c||/\sum|F_o|$, $R_w = [\sum w(|F_o| - |F_c|)^2/\sum wF_o^2]^{1/2}$.

2.4. Computational details

All calculations were carried out using GAUSSIAN-03 [14]. Ligand and complex structures were optimized using Becke's hybrid B3LYP functional [15]. The split-valence with polarization (SVP) basis set of Ahlrichs and coworkers [16] was felt to provide a good compromise between computational accuracy and efficiency, and was used for all calculations, except where noted. For all geometry optimizations, frequencies were also calculated to ensure that the structures were genuine minima on the potential energy hypersurface (no imaginary frequencies were found).

3. Results and discussion

3.1. Structures

3.1.1. $[Cu_2(L7)_2(C_2O_4)(H_2O)_2(NO_3)_2]$ (1)

The molecular structure of **1** is comprised of three similar dinuclear fragments, all involving the bidentate ligand 2-acetylpyridine hydrazone (L7), and a bridging oxalate. In combination they are represented by the averaged formula above. Relevant bond distances and angles are listed in Table 2. Two fragments are shown in Fig. 1(a). The Cu(3) fragment has four distant nitrates bound to a 'flat' dinuclear center, with long Cu–O contacts (Cu(3)–O(12) 2.524(4) Å, Cu(3)–O(14) 2.468(4) Å). Cu–L in plane distances fall in the range 1.973–1.985 Å, and the Cu–Cu distance is 5.149(3) Å. The bridging oxalate has a typical geometry. The Cu(3) dinuclear subunit is hydrogen bonded to the Cu(4) subunit (Fig. 1(a); O(15)–O(9) 2.795(5) Å, O(9)–O(13) 2.786(6) Å). Subunit Cu(4) has a similar geometry with five-coordinate square pyramidal copper centers, and with each metal having an axially bound water molecule (Cu(4)–O(9) 2.273(4) Å). The third dinuclear subunit (Fig. 1(b)) has a similar structure with square pyramidal copper centers, and axial contacts to oxygen atoms from a disordered combination of a water molecule and a nitrate (Cu(1)–O(21) 2.345(5) Å, Cu(2)–O(20) 2.365(5) Å). Other dimensions within this dinuclear subunit are similar to those involving Cu(3) and Cu(4).

3.1.2. L3

The structure of the ligand (L3) is shown in Fig. 2, and relevant bond distances and angles are listed in Table 3. The good refinement shows that a proton resides on N(2) and that the C–O bond has predominantly double bond character (C(6)–O(1) 1.230(5) Å). The N(2)–N(3) distance (1.389(5) Å) indicates this bond to have mostly single bond character. One interesting structural feature that bears on the reactivity of this ligand surrounds the *anti* (*trans*) conformation of the ligand as a whole, and in particular with respect to the two methyl groups, as indicated by the torsional angles C(10)–C(8)–C(7)–C(9) and C(7)–N(3)–N(2)–C(6) (177.4°, 178.1°, respectively), which are both very large. DFT calculations on L3, which utilize the B3LYP functional and 6-31G(d) basis set, indicate that the *anti* form

Table 2
Distances (Å) and angles (°) for $[Cu_2(L7)_2(C_2O_4)(H_2O)_2(NO_3)_2]$ (**1**)

Cu1–N1	1.965(5)
Cu1–N2	1.971(5)
Cu1–O2	1.974(4)
Cu1–O1	1.974(4)
Cu1–O21	2.346(5)
Cu2–N5	1.943(5)
Cu2–N4	1.975(5)
Cu2–O4	1.983(4)
Cu2–O3	1.983(4)
Cu2–O20	2.367(5)
Cu3–N7	1.968(5)
Cu3–O5	1.972(4)
Cu3–O6	1.973(4)
Cu3–N8	1.984(5)
Cu4–N10	1.970(5)
Cu4–O8	1.973(4)
Cu4–O7	1.985(5)
Cu4–N11	1.987(5)
Cu4–O9	2.273(4)
N1–Cu1–N2	82.0(2)
N1–Cu1–O2	173.75(19)
N2–Cu1–O2	95.80(19)
O6–Cu3–N8	95.0(2)
N10–Cu4–O8	97.6(2)
N10–Cu4–O7	168.6(2)
O8–Cu4–O7	84.91(18)
N10–Cu4–N11	81.2(2)
O8–Cu4–N11	170.21(19)
N1–Cu1–O1	96.87(19)
N2–Cu1–O1	175.23(18)
O2–Cu1–O1	84.84(16)
N1–Cu1–O21	91.3(2)
N2–Cu1–O21	94.28(19)
O2–Cu1–O21	94.72(17)
O1–Cu1–O21	90.38(18)
N5–Cu2–N4	81.7(2)
N5–Cu2–O4	175.2(2)
N4–Cu2–O4	99.62(19)
N5–Cu2–O3	93.5(2)
N4–Cu2–O3	172.54(19)
O4–Cu2–O3	84.75(16)
N5–Cu2–O20	90.7(2)
N4–Cu2–O20	95.0(2)
O4–Cu2–O20	93.82(18)
O3–Cu2–O20	90.71(18)
N7–Cu3–O5	98.4(2)
N7–Cu3–O6	176.7(2)
O5–Cu3–O6	84.74(18)
N7–Cu3–N8	81.8(2)
O5–Cu3–N8	179.3(2)
O7–Cu4–N11	94.4(2)
N10–Cu4–O9	99.26(18)
O8–Cu4–O9	91.20(16)
O7–Cu4–O9	91.82(16)
N11–Cu4–O9	98.58(17)

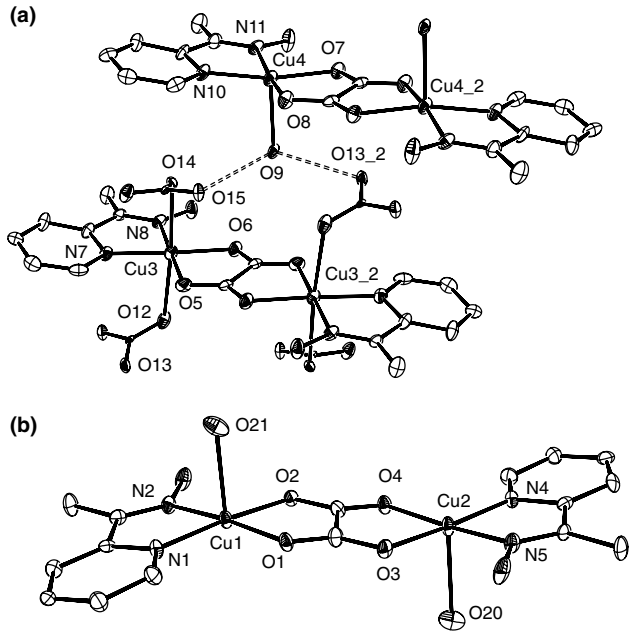

Fig. 1. (a) Structural representation of two dinuclear fragments in **1** (40% probability thermal ellipsoids). (b) Structural representation of a third dinuclear fragment in **1** (40% probability thermal ellipsoids).

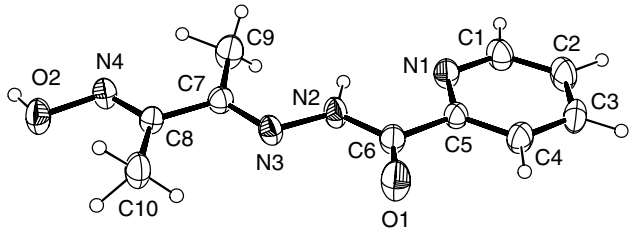

Fig. 2. Structural representation of L3 (40% probability thermal ellipsoids).

Table 3
Distances (Å) and angles (°) for L3

O1–C6	1.230(5)
O2–N4	1.408(5)
N1–C1	1.336(6)
N1–C5	1.342(5)
N2–N3	1.389(5)
N2–C6	1.332(6)
N3–C7	1.297(5)
N4–C8	1.291(6)
C1–C2	1.380(7)
C2–C3	1.372(8)
C4–C5	1.372(6)
C5–C6	1.501(6)
C7–C8	1.459(6)
C7–C9	1.490(7)
C8–C10	1.507(7)
C1–N1–C5	116.7(5)
N3–N2–C6	120.8(4)
N2–N3–C7	115.4(4)
O2–N4–C8	111.3(4)
N1–C1–C2	123.4(5)
C1–C2–C3	118.7(5)
C2–C3–C4	118.7(5)
C3–C4–C5	119.3(5)
N1–C5–C4	123.2(5)
N1–C5–C6	116.5(4)
C4–C5–C6	120.3(4)
O1–C6–N2	125.6(5)
O1–C6–C5	120.5(5)
N2–C6–C5	113.9(4)
N3–C7–C8	114.9(4)
N3–C7–C9	125.3(5)
C8–C7–C9	119.9(5)
N4–C8–C7	113.9(4)
N4–C8–C10	124.7(4)
C7–C8–C10	121.4(4)

is more stable than the *eclipsed* form, with an energy difference of ~25 kJ/mol.

3.1.3. [Ni(L8)]Br·CHCl$_3$ (3)

The molecular structure of **3** is shown in Fig. 3(a), and relevant bond distances and angles are given in Table 4. The obvious first point of discussion is the fact that the starting ligand (L3) is not present, but a new Schiff base ligand L8 is formed, based on a central butane-dione fragment. L8 acts in a tetradentate fashion coordinating to the nickel ion via two diazine nitrogen atoms, a pyridine nitrogen and an oxygen atom, creating quite a strong in plane crystal field. This is strong enough to cause the Ni(II) ion to be low spin (vide infra). The NiN_3O subunit is essentially planar (O(1)–Ni–N(5) 179.8(2)°, N(3)–Ni–N(6) 178.9(2)°), with very short Ni-ligand contacts (1.828–1.887 Å). Both C–O bonds have predominantly double bond character (C(6)–O(1) 1.285(6) Å, C(11)–O(2) 1.222(6) Å), and since the ligand has lost one proton, nitrogen atoms N(3) and N(5) bear a formal negative charge, consistent with the short Ni–N distances. The second proton (H(1)) resides on pyridine nitrogen N(1) (difference map), thus giving the complex ion a formal charge of 1+. The bromide ion (Br(1)) balances the charge, and is hydrogen bonded to H(1) and also to a chloroform molecule (Br(1)–H(16) 2.692(6) Å, Br(1)–H(1) 2.467(6) Å).

The flat nature of the Ni(II) ion, generated by the strong in plane crystal field, predisposes the whole ligand to adopt a fairly flat overall conformation, with the methyl groups in an unexpected *cis*-conformation (see structure of L3). The molecules are arranged in a stacked, alternating, *trans*-conformation in the lattice, with pairs of molecules related by an inversion centre. There are many relatively short (<4 Å) intermolecular contacts between individual molecules, e.g., N(4) and O(1) (3.304 Å) (highlighted in Fig. 3(b)), with the Ni–Ni distances between molecules in the stack alternating as 3.663(3), and 4.743(4) Å. Any axial contacts to the nickel centres between molecules are considered too weak to be of bonding significance. However, the intermolecular contacts are clearly instrumental in the parallel arrangement of the molecules of **3**. The complexes

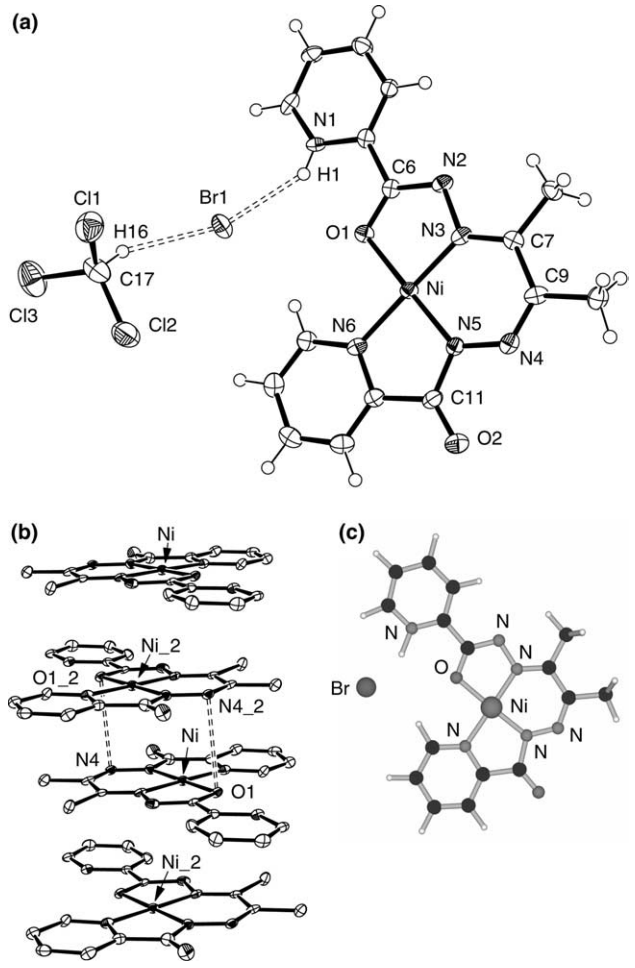

Fig. 3. (a) Structural representation of **3** (40% probability thermal ellipsoids). (b) Extended structural representation of **3** (40% probability thermal ellipsoids). (c) Optimized geometry for **3** (B3LYP/SVP).

Table 4
Distances (Å) and angles (°) for [Ni(L8)]Br·$CHCl_3$ (**3**)

Ni–N5	1.828(5)
Ni–N3	1.831(5)
Ni–O1	1.865(4)
Ni–N6	1.887(5)
N2–N3	1.397(7)
N4–N5	1.350(7)
N1–H1	0.80(9)
N5–Ni–N3	93.9(2)
N5–Ni–O1	178.8(2)
N3–Ni–O1	85.05(19)
N5–Ni–N6	85.4(2)
N3–Ni–N6	178.9(2)
O1–Ni–N6	95.61(19)
C6–O1–Ni	108.1(4)
C1–N1–C5	122.3(5)
C1–N1–H1	120(7)
C5–N1–H1	117(7)

$[Ni(L8)](ClO_4)\cdot H_2O$ and $[Ni(L8)](NO_3)\cdot 2H_2O$ are assumed to have similar overall structures.

Of note is the fact that the DFT structure (Fig. 3(c)) and X-ray structure (Fig. 3(a)) of [Ni(L8)]Br are in excellent agreement. For the square-planar nickel coordination sphere, the average deviation in bond lengths between the two structures was 0.02 Å. The average deviation in bond angles was 0.6°. This is comparable to results reported by Jang et al. [17] for the structures of iron carbonyls, where differences between B3LYP (double-ζ plus polarization basis set) and X-ray crystal structures were on the order of 0.02 Å and 0.5° for bond lengths and angles, respectively. For a medium-sized transition metal complex such as **3** (41 atoms, with 467 basis functions), such agreement is quite reasonable. This indicates the theory and basis set used are likely sufficient for the obtainment of good quality results.

3.1.4. $[Cu_2(L9)(L10)]\cdot 2H_2O\cdot CH_3OH\cdot L11$ (**4**)

The structure of the asymmetric unit in **4** is shown in Fig. 4, and relevant bond distances and angles are listed in Table 5. The original ligand L4 is clearly absent, and instead the complex contains three different ligand fragments derived from L4; the mono-acid ligand (L9), 4-chloro-2,6-pyridinedicarboxylate (L10) and 3-phenyltriazolo[1,5-a]pyridine (L11). Cu(1) and Cu(2) are bridged by the N–N diazine group in L9. A pyridine nitrogen (N(4)) and a carboxylate oxygen (O(2)) and the other pyridine nitrogen (N(1)) complete coordination to Cu(1). Cu(2) is bonded to the hydrazone oxygen O(1) from L9, and three donors (N(5), O(4), O(7)) from the dicarboxylate ligand L10. Cu(1) has four short in plane contacts (1.903–2.006 Å), but in the extended structure a fifth axial contact (Cu(1)–O(3) 2.632(3) Å) indicates that the geometry is axially elongated square-pyramidal (vide infra) (N(3)–Cu(1)–O(2) 162.2°, N(4)–Cu(1)–N(1) 173.4°). Cu(2) has a distorted square pyramidal coordination geometry within the asymmetric unit, with short in plane distances (1.903–2.033 Å), and a longer axial contact (N(2)–Cu(2) 2.368(3) Å). However, in the extended structure (vide infra) a sixth contact (Cu(2)–O(6) 2.375(2) Å) shows that the geometry is actually axially elongated octahedral. There are no anions in the structure indicating that both ligands have

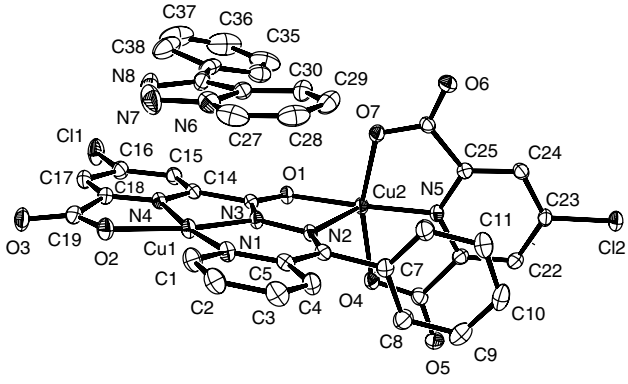

Fig. 4. Structural representation of the asymmetric unit in **4** (30% probability thermal ellipsoids).

Table 5
Distances (Å) and angles (°) for $[Cu_2(L9)(L10)]\cdot 2H_2O\cdot CH_3OH\cdot L11$ (**4**)

Cu1–N4	1.903(3)
Cu1–N1	1.922(3)
Cu1–N3	1.926(3)
Cu1–O2	2.005(2)
Cu2–N5	1.903(2)
Cu2–O1	1.971(2)
Cu2–O7	2.031(2)
Cu2–O4	2.033(2)
Cu2–N2	2.368(3)
Cu2–O6	2.375(2)
N2–N3	1.377(3)
N6–N7	1.359(5)
N7–N8	1.315(5)
N4–Cu1–N1	173.41(11)
N4–Cu1–N3	81.24(11)
N1–Cu1–N3	94.16(11)
N4–Cu1–O2	81.01(10)
N1–Cu1–O2	103.56(10)
N3–Cu1–O2	162.24(10)
N5–Cu2–O1	173.00(10)
N5–Cu2–O7	80.65(10)
O1–Cu2–O7	99.77(9)
N5–Cu2–O4	80.07(10)
O1–Cu2–O4	99.81(9)
O7–Cu2–O4	160.38(9)
N5–Cu2–N2	111.93(9)
O1–Cu2–N2	75.06(8)
O7–Cu2–N2	88.88(9)
O4–Cu2–N2	94.98(9)
N5–Cu2–O6	83.71(9)
O1–Cu2–O6	89.33(8)
O7–Cu2–O6	87.60(9)
O4–Cu2–O6	93.84(9)
N2–Cu2–O6	163.17(8)

lost two protons. This is consistent with the in plane Cu–O and Cu–N distances. The torsional angle Cu(1)–N(3)–N(2)–Cu(2) (178°) indicates an almost *trans* disposition of the copper atoms about the N–N single bond; however, this is an orthogonal magnetic connection (vide infra). The copper equatorial planes are also connected by a longer N–C–O pathway through N(3) and O(1).

A remarkable feature of the structure is the presence of the 'uncoordinated', fused triazole molecule L11. Fig. 4 shows that the phenyl triazole is held in place above three rings associated with the coordinated ligand L9. The pyridine ring is positioned above the N(1) pyridine ring in L9, the phenyl ring above the chloro-pyridine ring in L9 and the triazole ring above the chelate ring involving O(2) in L9. Distances between these rings subunits are relatively short (e.g., 3.3–4.0 Å) indicating that there are significant π-stacking interactions at play, which help to stabilize the location of the triazole molecule. The shortest distance (3.386 Å) is between N(7) and O(2). This is quite remarkable, possibly unprecedented in normal coordination chemistry, and highlights the importance of π stacking forces as a means of 'holding' a molecule in close proximity to a metal ion site. One is reminded of the unusual stabilization of a tryptophan moiety close to the active site in galactose oxidase, with a possibly similar interaction with a tyrosine ligand [18]. Also the phenyl ring of L9 is positioned above the pyridine ring (N(5)) in L11, with short contacts between ring atoms (3.45–3.77 Å) highlighting the nice fit of the aromatic rings in this complex.

The overall structure of **4** reveals some further surprises. The dinuclear subunit shown in Fig. 4 actually forms a dimer through a carboxylate bridge (O(6)) linking Cu(2) with its symmetry related counterpart. Also, the tetranuclear subunits are cross-linked to form a zig-zag chain, via symmetry related O(6) atoms (Fig. 5), and finally the zig-zag chains are cross-linked into a 2D grid by long axial O(3)–Cu(1) contacts (2.632(3) Å) shown in Fig. 6. The global direct connectivity between the copper atoms in all cases links the metal ions orthogonally, thus predisposing the system

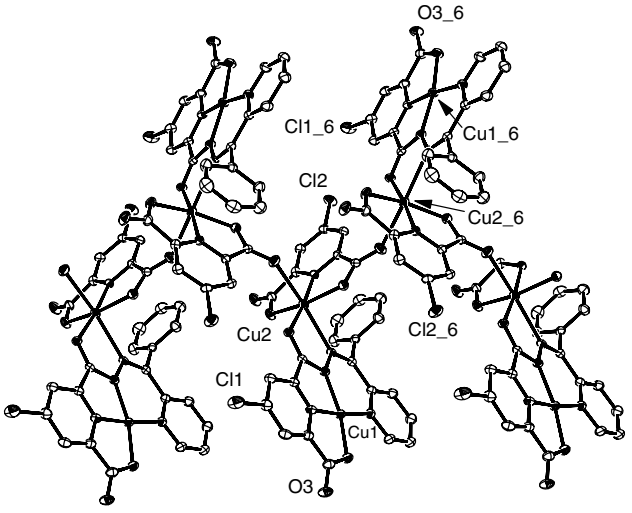

Fig. 5. Structural representation of the chain motif in **4** (30% probability thermal ellipsoids).

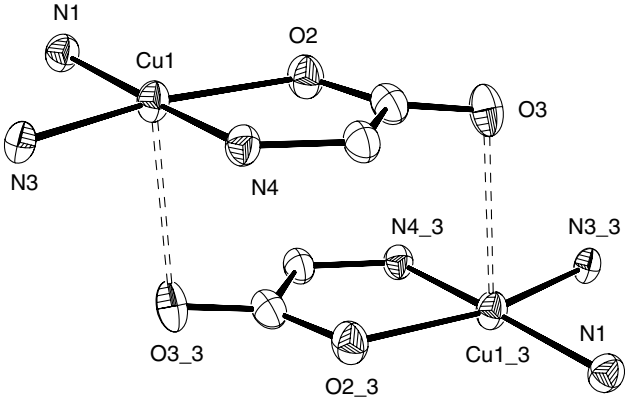

Fig. 6. Extended cross linked structural representation of the chains in **4** (40% probability thermal ellipsoids).

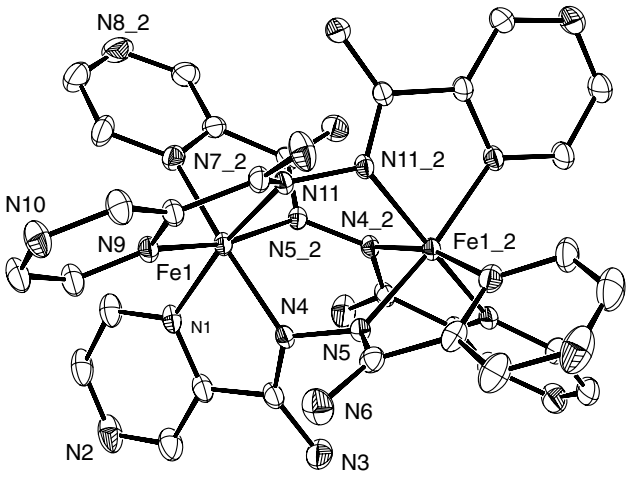

Fig. 7. Structural representation of **5** (40% probability thermal ellipsoids).

to the absence of significant antiferromagnetic exchange (vide infra).

3.1.5. $[Fe_2(PZHPZ)_3](ClO_4)_4\cdot 2CH_3CN$ (**5**)

The molecular structure of **5** is shown in Fig. 7, and relevant bond distances and angles are listed in Table 6. L5 is clearly absent and the simple pyrazine amidrazone ligand is involved in coordination to Fe(II). Three ligands are wrapped around the two iron(II) centers in a spiral fashion, with three single N–N bonds connecting the metal ions. The dinuclear complex cation is essentially identical to that reported previously for the complex $[Fe_2(PZHPZ)_3](NO_3)_4\cdot 5H_2O$ [2], obtained from the reaction of $Fe(NO_3)_3$ with PZHPZ (Chart 1), with slight differences in internal dimensions. Fe–N distances

Table 6
Distances (Å) and angles (°) for $[Fe_2(PZHPZ)_3](ClO_4)_4\cdot 2CH_3CN$ (**5**)

Fe1–N9	1.958(3)
Fe1–N1	1.963(3)
Fe1–N11	1.964(3)
Fe1–N5	1.964(3)
Fe1–N4	1.968(3)
Fe1–N7	1.971(3)
N4–N5	1.412(4)
N11–N11	1.409(5)
N9–Fe1–N1	95.86(12)
N9–Fe1–N11	79.92(12)
N1–Fe1–N11	167.86(13)
N9–Fe1–N5	167.53(12)
N1–Fe1–N5	95.87(12)
N11–Fe1–N5	89.38(11)
N9–Fe1–N4	97.49(12)
N1–Fe1–N4	79.65(12)
N11–Fe1–N4	89.56(12)
N5–Fe1–N4	88.76(11)
N9–Fe1–N7	95.19(13)
N1–Fe1–N7	94.84(13)
N11–Fe1–N7	96.87(12)
N5–Fe1–N7	79.62(12)
N4–Fe1–N7	166.62(13)

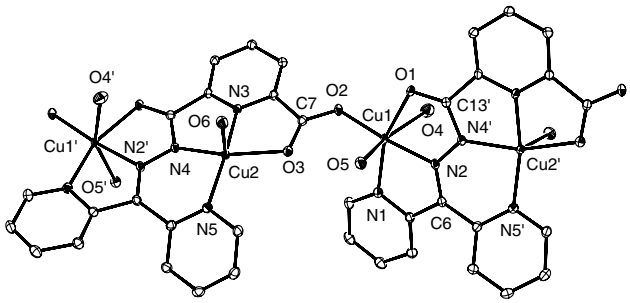

Fig. 8. Structural representation of **6** (40% probability thermal ellipsoids).

in **5** are slightly longer (1.961–1.970 Å) in keeping with a slightly larger Fe–Fe separation (3.621(3) Å). Torsional angles (Fe–N–N–Fe) are very small (43.8°) indicating an acute arrangement of Fe–N bonds about the N–N single bonds (N–N 1.411–1.413 Å). The generally short Fe–N distances are indicative of a strong ligand field for Fe(II), consistent with the low spin nature of this compound (vide infra).

3.1.6. $[Cu_2(L12\text{-}2\,H)](NO_3)_2\cdot 1.5H_2O$ (**6**)

The structure of **6** is shown in Fig. 8, and relevant bond distances and angles are listed in Table 7. The structure reveals that the starting ligand (L6) has been hydrolysed at the hydrazide function during the reaction

Table 7
Distances (Å) and angles (°) for $[Cu_2(L12\text{-}2H)](NO_3)_2\cdot 1.5H_2O$ (**6**)

Cu1–O2	1.9168(13)
Cu1–N2	1.9410(15)
Cu1–N1	2.0213(14)
Cu1–O1	2.0935(12)
Cu1–O4	2.4079(14)
N2–N4	1.346(2)
Cu2–N3	1.9419(14)
Cu2–N4	1.9427(14)
Cu2–N5	1.9822(14)
Cu2–O3	2.1002(12)
Cu2–O6	2.1771(13)
O2–Cu1–N2	174.14(6)
O2–Cu1–N1	103.86(5)
N2–Cu1–N1	79.41(6)
O2–Cu1–O1	96.49(5)
N2–Cu1–O1	80.18(5)
N1–Cu1–O1	159.59(5)
O2–Cu1–O4	94.34(5)
N2–Cu1–O4	80.35(6)
N1–Cu1–O4	97.29(6)
O1–Cu1–O4	79.47(5)
N3–Cu2–N4	79.52(6)
N3–Cu2–N5	165.47(6)
N4–Cu2–N5	90.72(6)
N3–Cu2–O3	78.96(5)
N4–Cu2–O3	155.74(5)
N5–Cu2–O3	108.03(5)
N3–Cu2–O6	97.21(5)
N4–Cu2–O6	107.92(6)
N5–Cu2–O6	96.02(5)
O3–Cu2–O6	85.81(5)

with copper nitrate in aqueous methanol to form the corresponding acid. The individual carboxylate ligands result in the formation of a 1D chain, with dinuclear subunits. Each ligand coordinates in a heptadentate fashion binding to Cu(1) via two pyridine nitrogen atoms, one diazine nitrogen atom and a carboxylate oxygen, and to Cu(2) via pyridine and diazine nitrogen atoms, and a terminal hydrazone oxygen. The square-pyramidal Cu(2) coordination sphere is completed by an axial water molecule (Cu(2)–O(6) 2.177(2) Å), and two axial water molecules complete the Jahn–Teller distorted six-coordinate Cu(1) (Cu(1)–O(4) 2.408(1) Å; Cu(1)–O(5) 2.480(1) Å). The chain is propagated by *syn–anti* carboxylate bridging between the dinuclear subunits through oxygen O(2), which binds equatorially to both Cu(1) and Cu(2). The Cu(1)′–N(2)′–N(4)–Cu(2) torsional angle (164.7°) indicates an almost *trans* disposition of the copper basal planes relative to the N–N bridge (Cu(1)–Cu(2)′ 4.683(2) Å). The *syn–anti* carboxylate bridge leads to a much larger metal ion separation (Cu(1)–Cu(2) 5.336(2) Å).

The presence of two nitrate anions per dinuclear subunit indicates that the ligand has lost two protons. The carboxylate is clearly one site of deprotonation. Establishing the other site of deprotonation depends on a clear identification of the bond order within the C(6)–N(2)–N(4)′–C(13)′–O(1) framework (bond distances 1.301, 1.346, 1.354, 1.249 Å, respectively). This is difficult, and is complicated by very short Cu(1)–N(2) and Cu(2)′–N(4)′ distances (1.941(2), 1.943(1) Å, respectively). One could safely conclude that the charge is delocalized within this bridging ligand framework.

3.1.7. [Ni(L4-2H)] (7)

The molecular structure of **7** is shown in Fig. 9, and important distances and angles are listed in Table 8. The complex consists of one full ligand (L4) bonded to a single four coordinate Ni(II) center, via pyridine nitrogen atoms N(1) and N(4), and diazine nitrogen atoms N(3) and N(5). The Ni–N distances are very short (1.82–1.91 Å), typical of square planar Ni(II), but the nickel geometry has a slight tetrahedral distortion (N(3)–Ni(1)–N(5) 164°, N(1)–Ni(1)–N(4) 159°). No anions are present and so the ligand bears a 2− charge. C–O distances are very short (C(13)–O(1) 1.232(7) Å, C(19)–O(2) 1.222(7) Å), indicating them to have double bond character. The sites of deprotonation are, therefore, reasonably assigned to N(3) and N(5). There are no close contacts of significance between individual molecules in the lattice.

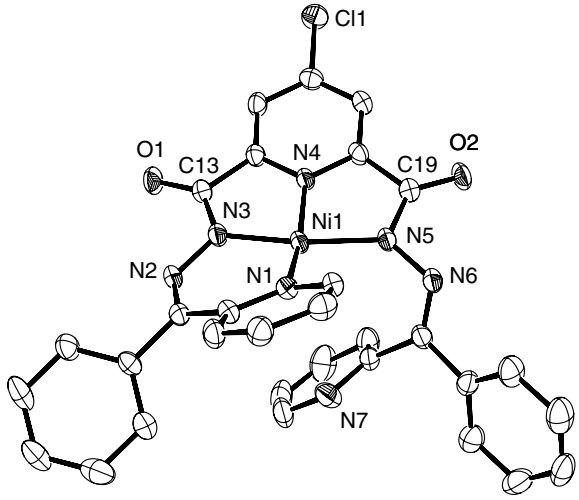

Fig. 9. Structural representation of **7** (40% probability thermal ellipsoids).

Table 8
Distances (Å) and angles (°) for [Ni(L4-2H)] (**7**)

Ni1–N1	1.906(5)
Ni1–N3	1.843(5)
Ni1–N4	1.822(5)
Ni1–N5	1.930(5)
N2–N3	1.378(7)
N5–N6	1.411(7)
N1–Ni1–N3	94.0(2)
N1–Ni1–N4	159.4(2)
N1–Ni1–N5	102.1(2)
N3–Ni1–N4	83.7(3)
N3–Ni1–N5	163.7(2)
N4–Ni1–N5	81.8(3)

3.2. Ligand decomposition reactions

L2 was prepared by the reaction of diethyl oxalate with hydrazine, followed by the reaction of the dihydrazide with 2-acetylpyridine. The production of 2-acetylpyridine hydrazone (L7) and oxalate on reaction with $Cu(NO_3)_2$ in aqueous methanol indicates ligand hydrolysis at the oxalate imine sites rather than the acetyl imine sites. Pre-coordination of two copper(II) ions to the ligand (e.g., as in Scheme 2) would lead to Lewis acid promoted nucleophilic attack by water at the oxalate C=N sites, thus producing oxalate, which could then simply bridge the two copper centers. The 2-acetylpyridine hydrazone could then pivot about the pyridine–copper bond to assume its coordination role as indicated in the structure of **1**. A similar hydrolytic decomposition appears to have occurred for **2**. It is of interest to note that this ligand forms a stable tetranuclear Ni(II) complex $[Ni_4(L2)_4](BF_4)_4 \cdot 6H_2O$, with no evidence of ligand decomposition [19].

The ligand in **3** (L8), produced from the reaction of L3 with $NiBr_2$, would be expected as the product from the direct reaction of butane-2,3-dione and 2-picolinic acid hydrazide. However, ligand L3 was derived from butanedione monoxime, and was characterized by

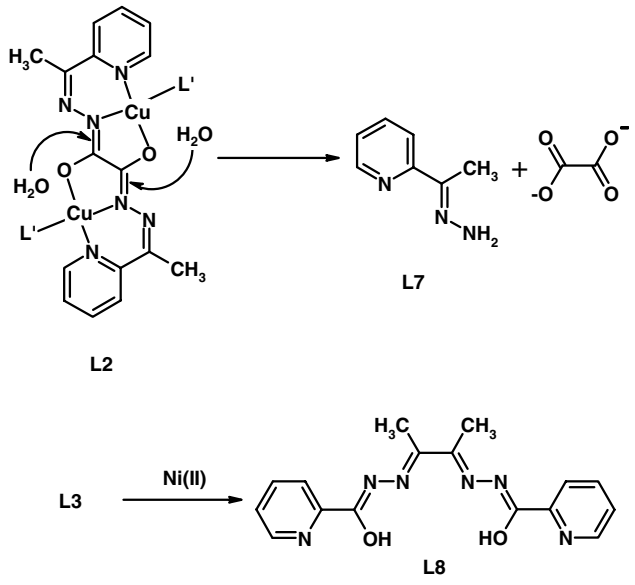

Scheme 2.

X-ray crystallography so leaving little doubt as to its identity (Scheme 2). In our hands L3 was found to be fairly unreactive to transition metal salts in general, and this was attributed in part to the *anti* conformation of the ligand itself (Fig. 2), which would probably impede the simultaneous coordination of the pyridine and oxime ends of the ligand.

In order for L3 to bind to a metal ion in a chelating fashion a significant energy expenditure (vide supra) would be required to bring suitable donor groups into an appropriate chelating conformation. Two reasonable chelation isomers are possible on reaction with nickel bromide (Fig. 10(a) and (b); Br is proposed as a co-ligand), of which the oxime N-bonded example (a) is the more stable than (b) by 86 kJ mol^{-1}. With this isomer, polarization of both C=N bonds in L3 would occur, and so would provide a hydrolytic mechanism by which both picolinic hydrazide and the methyl ketone shown in Fig. 10 (c) could be released prior to reaction to form L8. It is of interest to note that reaction of L3 with other Ni(II) salts also produced red diamagnetic complexes of L8 (e.g., $[Ni(L8)](ClO_4)\cdot H_2O$ and $[Ni(L8)](NO_3)\cdot 2H_2O$), and it is reasonable to assume that they are all produced by the same hydrolytic process. The square planar Ni(II) complex (**3**) was calculated to be 30 kJ mol^{-1} more stable than the initially proposed [Ni(L3)Br] chelate (Fig. 10(a)). Since the same ligand rearrangement was observed with several nickel salts, it suggests that this might be the overall driving force for the hydrolytic process.

A recent report indicates that complexes of L3 with Cr(III), Fe(III), Co(II), Ni(II), Cu(II), Zn(II), Cd(II) and UO_2^{2+} can be produced by refluxing the ligand with the appropriate metal salt in ethanol. No evidence for ligand decomposition was presented, and no structures were reported. It is of interest to note that a diamagnetic orange nickel(II) complex, [Ni(L3-H)Cl], was discussed [3].

L4 is part of a growing group of tritopic ligands based on a central 2,6-picolinic dihydrazide framework, which form predominantly $[M_9(\mu\text{-}O)_{12}]$ $[3\times3]$ grid structures [20–26]. A similar ligand (L4′) (Chart 1, L4; R = H) appears to be quite stable in its reaction with Mn(II) salts, and the complex $[Mn_9(L4')_6](NO_3)_6\cdot 12H_2O$ has been produced in a reasonable yield, and shown to have a $[Mn_9(\mu\text{-}O)_{12}]$ $[3\times3]$ grid structure by single crystal X-ray diffraction [26]. However, reaction of L4 with copper acetate in methanol in the presence of air produces as the main product complex **4**. The formation of the mono-carboxylate ligand L9, and the dicarboxylate ligand L10 clearly results from a 'reverse hydrolysis' reaction in which the full hydrazone ligand L4 has undergone nucleophilic attack by water at the 2,6-pyridine dicarboxylic acid sites, rather than at the Schiff base imine positions (Scheme 3). This is presumably encouraged by the pre-coordination of L4 to Cu(II), at least in the central pyridine cavity, although it is highly likely that the pre-coordination involves a trinuclear copper(II) complex, similar to other linear $Cu(II)_3$ complexes observed with this class of ligand [25,27].

Perhaps the most surprising result is the formation of the triazole derivative 3-phenyl-triazolo[1,5-a]pyridine (L11). It is of interest to note that the 2-pyridyl analogue 3-(2-pyridyl)-triazolo[1,5-a]pyridine is produced by the reaction of di-2-pyridyl ketone and hydrazine hydrate in methanol–water (1:1) in the presence of air [28], or by the oxidation of di-2-pyridyl ketone hydrazone with nickel(II) peroxide in benzene [29]. It also appears to have resulted from a reaction between a di-2-pyridyl

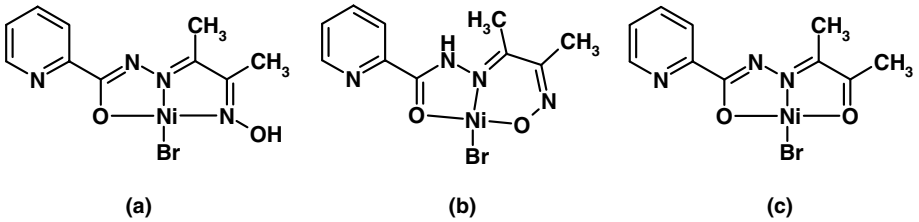

Fig. 10. Chelation isomers for L3 (a,b) and proposed hydrolysis product (c).

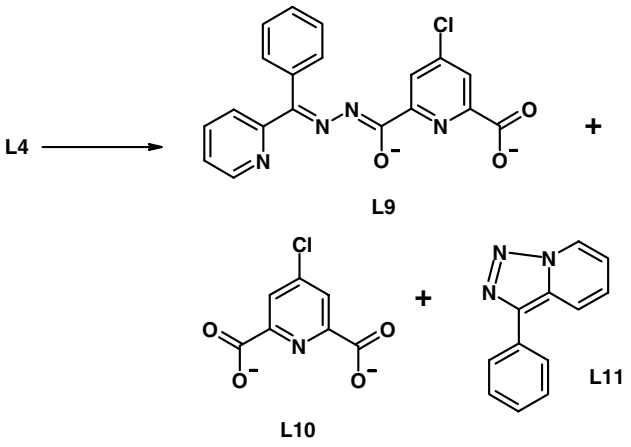

Scheme 3.

ketone hydrazone and copper nitrate in air via an oxidative cyclization, producing the copper(II) complex of the triazole [28]. The hydrazone of 2-benzoyl pyridine can also be oxidatively cyclized to the corresponding triazole 3-phenyl-triazolo[1,5-a]pyridine, by reaction with silver oxide [30]. The simultaneous formation of the mono- and di-acid ligands (L9, L10) suggests that phenyl-2-pyridyl ketone hydrazone is formed first, which then oxidatively cyclizes under mild conditions in the presence of air to produce L11. This process may be catalyzed by the presence of Cu(II) ions.

L4 reacts with cobalt(II) nitrate in CH_3CN/CH_3OH in air to form the complex $[(L4)_3(L9)_6Co(III)_6Co(II)_6(H_2O)_6(NO_3)_6]$ $[Co(H_2O)_6](NO_3)_8(CH_3CN)_3(H_2O)_6$ (**8**), which contains both L4 and L9, and has been reported previously [31]. Two views are shown in Figs. 11(a) and (b) looking down the trigonal axis of the molecule, and from a side view, respectively. The mono-carboxylate ligand L9 binds six metal ions on each trigonal face, with three Co(2) (Co(II)) atoms bridged by *syn–anti* carboxylates in an inner triangular array, with hydrazone oxygen atoms bridging each of them to the outer Co(1) (Co(III)) centers. The Co(1) centers are linked by the two end N_2O pockets of the tritopic ligands L4 to form the dodecanuclear array. The thirteenth cobalt(II) ion appears in the lattice in part to balance the overall charge. There is no evidence to suggest the formation of the di-acid (L10) or the triazole (L11), but again this reaction serves to illustrate the hydrolytic instability of the hydrazone function in this class of ligand.

The formation of the carboxylate ligand L9 from L4 on reaction with $Co(NO_3)_2$ underlines the hydrolytic instability of the hydrazone linkages and the fact that Co(II) is capable of mediating nucleophilic attack at the imine site. The presence of Co(II) at the carboxylate site is a surprise since Co(III) would be expected to be more highly polarizing and to prefer the oxygen rich environment generated in the internal trigonal core. In

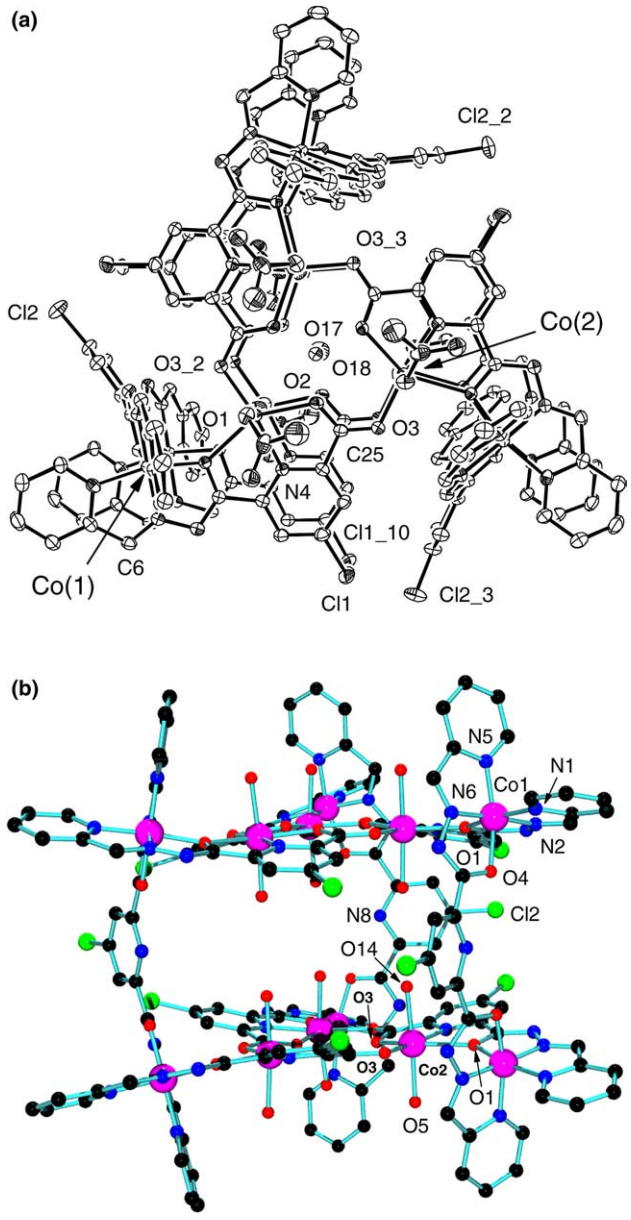

Fig. 11. (a) Structural representation of **8** viewed down the threefold symmetry axis (4% probability thermal ellipsoids), with phenyl rings removed for clarity. (b) Structural representation of **8** viewed at 90° to the threefold symmetry axis (POVRAY ©image).

view of the fact that no ligand decomposition occurs in the reaction between $NiCO_3$ and L4, this suggests that Co(III) is instrumental in the formation of L9.

The formation of the Fe(II) complex **5** containing the bis-bidentate ligand PZHPZ (Chart 1) from L5 (Scheme 4) is somewhat surprising, and indicates a different ligand decomposition mechanism. In this case any water involved in the hydrolysis must have arisen mostly from the hydrated metal salt itself, since CH_3CN was used as the solvent. This type of ligand contains amidrazone fragments at the ends, which are produced by reaction of, e.g., a picolinic-dihydrazide with the

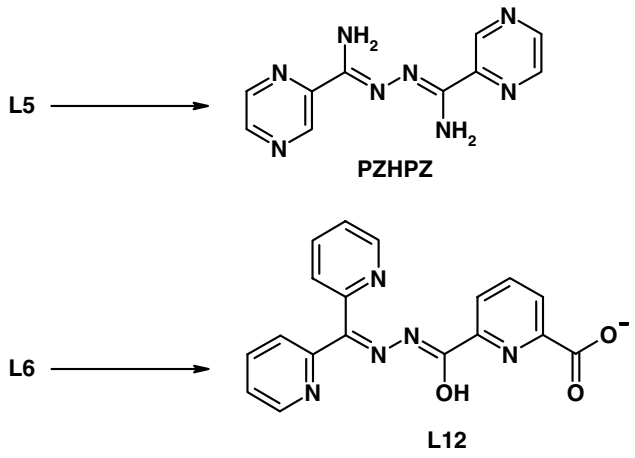

Scheme 4.

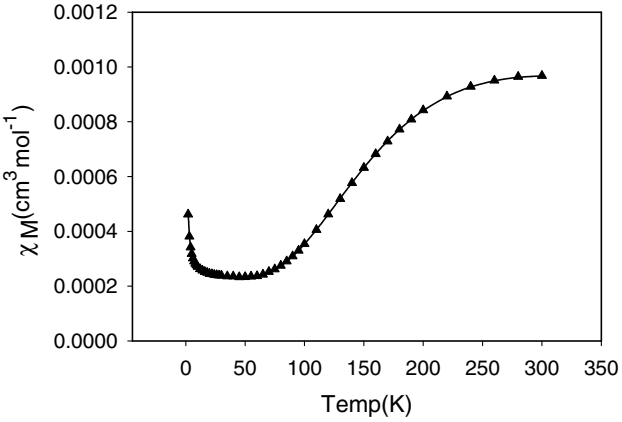

Fig. 12. Variable temperature magnetic data for **1**. The solid line represents the best fit result to Eq. (1) (see text for fitted parameters).

methylimidate ester derived from 2-cyanopyridine or 2-cyanopyrazine. Direct synthesis of PZHPZ can be achieved in high yield by the reaction of 2-pyrazinamide hydrazone with 2-pyrazine methylimidate [2]. It seems reasonable to assume that a reverse hydrolytic step has occurred in the reaction of L5 with a metal ion, in which the appropriate amidrazone is produced as one product by hydrolysis of the imine linkage adjacent to the central pyridine ring. It seems highly unlikely that the appropriate imidate would be produced as well, raising the question as to how PZHPZ is produced. The elimination of a hydrazine molecule between two condensing amidrazone moieties seems unlikely, but perhaps the formation of an amide by metal ion promoted hydrolysis at the peripheral imine C=N group could lead to a more simple metal ion facilitated condensation to produce PZHPZ.

L6 undergoes a simple hydrolysis reaction at the hydrazide carbonyl group on reaction with Cu(II) in aqueous methanol to produce the corresponding carboxylic acid (Scheme 4). This presumably is effected by pre-coordination of the Cu(II) ion to the hydrazide group first, which would polarize the carbonyl group and enhance electrophilic attack by water at the carbon atom.

3.3. Magnetic properties

The variable temperature magnetic properties of **1** show a rise in susceptibility with increasing temperature to a maximum around 300 K (Fig. 12), indicating significant intramolecular antiferromagnetic exchange. The low temperature increase corresponds to the presence of paramagnetic impurity. Given the structure of **1**, with essentially isolated oxalate bridged dinuclear copper(II) species, the data were fitted to a simple exchange expression for two interacting $S = 1/2$ centres ($H_{ex} = -2J\{S_1 \cdot S_2\}$) adapted for a paramagnetic impurity fraction (ρ), Weiss-like temperature correction (θ) and temperature independent paramagnetism ($N\alpha$) (Eq. (1)). A good fit gave $g = 2.21(1)$, $J = -171.5(4)$ cm^{-1}, $\rho = 0.0011$, $\theta = 0$ K, $N\alpha = 200 \times 10^{-6}$ cm^3 mol^{-1}

$$\chi_M = \frac{2Ng^2\beta^2}{k(T-\theta)}\left[\frac{1}{(3+\exp(-2J/kT))}\right](1-\rho) + \left(\frac{Ng^2\beta^2}{4kT}\right)\rho + N\alpha \quad (1)$$

($10^2R = 0.41$; $R = [\sum(\chi_{obs.} - \chi_{calc.})^2 / \sum \chi^2_{obs.}]^{1/2}$). The solid line in Fig. 12 was calculated with these parameters. The large singlet–triplet splitting (343 cm^{-1}) in this case is typical for oxalate bridged di-copper(II) complexes [32]. Compound **2** gave an essentially identical profile of susceptibility as a function of temperature, and fitting of the data to Eq. (1) gave $g = 2.24(4)$, $J = -172(8)$ cm^{-1}, $\rho = 0.0075$, $\theta = -0.2$ K, $N\alpha = 134 \times 10^{-6}$ cm^3 mol^{-1} ($10^2R = 1.7$). This clearly indicates the structural similarity between **1** and **2**, and oxalate bridging.

Complex **3** is diamagnetic, consistent with the square planar structure and the strong in plane ligand field. The corresponding nitrate and perchlorate complexes are also diamagnetic. Complex **7** is also diamagnetic, consistent with its square-planar structure. The variable temperature magnetic properties of **4** show that the magnetic moment is essentially constant between 2 and 300 K (2.9–3.2 μ_B/mol), indicative of essentially isolated spin centers. This is consistent with the structure, which shows a strictly orthogonal connection between Cu(1) and Cu(2) through the diazine (N–N) bridge. The long equatorial, non-orthogonal connection between Cu(1) and Cu(2) via N(3) and O(1) clearly does not lead to any significant spin exchange.

Complex **5** is essentially diamagnetic from 2 to 300 K, indicative of a low spin Fe(II) system, and identical to the behaviour of the iso-structural complex $[Fe_2(PZHPZ)_3](NO_3)_4$ [2]. The chain structure of **6** creates an alternating bridging arrangement between

the copper ions with N–N and *syn–anti* carboxylates connecting the copper magnetic orbitals directly. The presence of a direct *trans* diazine bridge with a large Cu–N–N–Cu torsional angle (164.7°) would suggest quite strong antiferromagnetic exchange [33], while the *syn–anti* carboxylate bridge would not be expected to generate significant exchange [34,35]. Variable temperature magnetic data (Fig. 13) show molar susceptibility reaching a maximum at ~200 K, indicating quite strong antiferromagnetic exchange coupling between the copper centres. Given the likely dominance of the diazine bridge in the exchange process, the data were fitted to Eq. (1), giving $g = 2.20(3)$, $2J = -234(2)\ \mathrm{cm}^{-1}$, $\theta = 1.4\ \mathrm{K}$, $\rho = 0.027$, $N\alpha = 120 \times 10^{-6}\ \mathrm{cm}^3\ \mathrm{mol}^{-1}$ ($10^2R = 3.3$; $R = [\sum(\chi_{\mathrm{obs.}} - \chi_{\mathrm{calc.}})^2/\sum\chi_{\mathrm{obs.}}{}^2]^{1/2}$). The solid line in Fig. 13 is calculated with these fitted parameters. This result is entirely consistent with *trans* N–N bridge connecting Cu(1) and Cu(2) [33]. The small positive θ correction might be considered to arise from the *syn–anti* carboxylate bridge, since the chains are well separated in the extended structure.

The dodecanuclear cobalt complex **8** actually contains thirteen cobalt ions ($Co(III)_6Co(II)_7$), with the $[Co(II)(H_2O)_6]^{2+}$ ion residing in the lattice. The variable temperature magnetic data show a slight variation in moment from 11.0 μ_B at 300 K to 10.2 μ_B at 100 K, followed by a smooth decrease to 8.5 μ_B at 2 K. The gradual drop in moment is indicative of possible weak intra-molecular antiferromagnetic exchange, but because of the complexities involved with fitting magnetic data for Co(II) systems in general no attempt has been made to evaluate an exchange integral. The *syn–anti* carboxylate triangular bridging arrangement of the Co(II) centres would not be expected to lead to significant coupling, which is consistent with the observed data [34,35]. This arises from a mismatch of the metal orbitals in the case of copper, which would be expected to have a similar effect in the present situation, in addition to the long distances of separation of the Co(II) centres (5.180 Å).

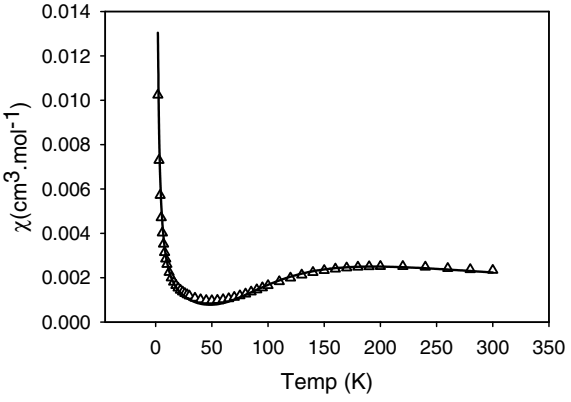

Fig. 13. Variable temperature magnetic data for **6**. The solid line represents the best fit result to Eq. (1) (see text for fitted parameters).

4. Conclusions

Seemingly innocent ligands, based on condensed hydrazone derivatives, have been shown to undergo some unexpected hydrolytic decomposition reactions in the presence of transition metal ions, with some fragments re-arranging to new ligands and some being incorporated into novel complex structures. In one most unusual case oxidatively cyclized 3-phenyl-triazolo [1,5a]-pyridine (L11) is trapped in a complex structure via extensive aromatic π interactions only, but is not coordinated. In another case a novel dodecanuclear Co(II)/Co(III) cluster is produced by the fortuitous combination of a hydrolyzed mono-carboxylate ligand with a complete dihydrazone ligand. In most cases the products can only be successfully characterized by an X-ray structural determination.

5. Supplementary data

Crystallographic data for the structural analyses have been deposited with the Cambridge Crystallographic Data Centre, CCDC reference numbers 237242–237247, 254194 for **1**, **3**–**7**, L3, respectively. Copies of this information may be obtained free of charge from the Director, CCDC, 12 Union Road, Cambridge, CB2 1EZ, UK (fax: +44 1223 336033; e-mail: deposit@ccdc.cam.ac.uk or www: http://www.ccdc.cam.ac.uk).

Acknowledgements

We thank NSERC (Natural Sciences and Engineering Research Council of Canada), the Research Council of Norway (HG), and EPSRC (JAKH) for financial support, and Dr. R. McDonald, University of Alberta, for structural data.

References

[1] Z. Xu, L.K. Thompson, D.O. Miller, E. Ruiz, S. Alvarez, Inorg. Chem. 42 (2003) 1107.
[2] Z. Xu, L.K. Thompson, D.O. Miller, H.J. Clase, J.A.K. Howard, A.E. Goeta, Inorg. Chem. 37 (1998) 3620.
[3] T.H. Rakha, Trans. Met. Chem. 24 (1999) 659.
[4] L.K. Thompson, L. Zhao, Z. Xu, D.O. Miller, W.M. Reiff, Inorg. Chem. 24 (2003) 128.
[5] (a) G.M. Sheldrick, SHELX-97, 1997;
(b) SIR-97: A. Altomare, M. Cascarano, C. Giacovazzo, A. Guagliardi, J. Appl. Crystallogr. 26 (1993) 343.
[6] P.T. Beurskens, G. Admiraal, G. Beurskens, W.P. Bosman, R. de Gelder, R. Israel, J.M.M. Smits, The DIRDIF-94 program system,

Technical Report of the Crystallography Laboratory, University of Nijmegen, The Netherlands, 1994.
[7] D.T. Cromer, J.T. WaberInternational Tables for X-ray Crystallography IV, vol. IV, The Kynoch Press, Birmingham, England, 1974, Table 2.2 A.
[8] J.A. Ibers, W.C. Hamilton, Acta Crystallogr. 17 (1964) 781.
[9] D.C. Creagh, W.J. McAuley, in: A.J.C. Wilson (Ed.), International Tables for Crystallography, vol. C, Kluwer Academic Publishers, Boston, 1992, pp. 219–222, Table 4.2.6.8.
[10] teXsan for Windows: Crystal Structure Analysis Package, Molecular Structure Corporation, 1997.
[11] J. Cosier, A.M. Glazer, J. Appl. Crystallogr. 19 (1986) 105.
[12] (a) Siemens. SMART Data Collection Software, Ver. 4.050; Siemens Analytical X-ray Instruments Inc., Madison, WI, 1996;
(b) Siemens. SAINT Data Reduction Software, Version 4.050; Siemens Analytical X-ray Instruments Inc., Madison, WI, 1996.
[13] Sheldrick, G.M., SHELXTL 5.04/VMS, An integrated system for solving, refining and displaying crystal structures from diffraction data. Siemens Analytical X-ray Instruments Inc., Madison, WI, 1995.
[14] M.J. Frisch, G.W. Trucks, H.B. Schlegel, G.E. Scuseria, M.A. Robb, J.R. Cheeseman, J.A. Montgomery Jr., T. Vreven, K.N. Kudin, J.C. Burant, J.M. Millam, S.S. Iyengar, J. Tomasi, V. Barone, B. Mennucci, M. Cossi, G. Scalmani, N. Rega, G.A. Petersson, H. Nakatsuji, M. Hada, M. Ehara, K. Toyota, R. Fukuda, J. Hasegawa, M. Ishida, T. Nakajima, Y. Honda, O. Kitao, H. Nakai, M. Klene, X. Li, J.E. Knox, H.P. Hratchian, J.B. Cross, C. Adamo, J. Jaramillo, R. Gomperts, R.E. Stratmann, O. Yazyev, A.J. Austin, R. Cammi, C. Pomelli, J.W. Ochterski, P.Y. Ayala, K. Morokuma, G.A. Voth, P. Salvador, J.J. Dannenberg, V.G. Zakrzewski, S. Dapprich, A.D. Daniels, M.C. Strain, O. Farkas, D.K. Malick, A.D. Rabuck, K. Raghavachari, J.B. Foresman, J.V. Ortiz, Q. Cui, A.G. Baboul, S. Clifford, J. Cioslowski, B.B. Stefanov, G. Liu, A. Liashenko, P. Piskorz, I. Komaromi, R.L. Martin, D.J. Fox, T. Keith, M.A. Al-Laham, C.Y. Peng, A. Nanayakkara, M. Challacombe, P.M.W. Gill, B. Johnson, W. Chen, M.W. Wong, C. Gonzalez, J.A. Pople, GAUSSIAN-03, Revision B.05, Gaussian, Inc., Pittsburgh PA, 2003.
[15] A.D. Becke, J. Chem. Phys. 98 (1993) 5648.
[16] A. Schaefer, H. Horn, R. Ahlrichs, J. Chem. Phys. 97 (1992) 2571.
[17] J.H. Jang, J.G. Lee, H. Lee, Y. Xie, H.F. Schaefer, J. Phys. Chem. A 102 (1998) 5298.
[18] N. Ito, S.E.V. Phillips, C. Stevens, Z.B. Ogel, M.J. McPherson, J.N. Keen, K.D.S. Yadav, P.F. Knowles, Nature 350 (1991) 87.
[19] L. Zhao, V. Niel, L.K. Thompson, Z. Xu, V.A. Milway, R.G. Harvey, D.O. Miller, C. Wilson, M. Leech, J.A.K. Howard, S.L. Heath, J. Chem. Soc., Dalton Trans. (2004) 1446.
[20] L. Zhao, C.J. Matthews, L.K. Thompson, S.L. Heath, Chem. Commun. (2000) 265.
[21] L. Zhao, Z. Xu, L.K. Thompson, S.L. Heath, D.O. Miller, M. Ohba, Angew. Chem. Int. Ed. 39 (2000) 3114.
[22] O. Waldmann, R. Koch, S. Schromm, P. Müller, L. Zhao, L.K. Thompson, Chem. Phys. Lett. 332 (2000) 73.
[23] O. Waldmann, L. Zhao, L.K. Thompson, Phys. Rev. Lett. 88 (2002) 066401-1-4.
[24] L. Zhao, Z. Xu, L.K. Thompson, D.O. Miller, Polyhedron 20 (2001) 1359.
[25] Z. Xu, L.K. Thompson, D.O. Miller, Polyhedron 21 (2002) 1715.
[26] L. Zhao, Z. Xu, H. Grove, V.A. Milway, L.N. Dawe, T.S.M. Abedin, L.K. Thompson, T.L. Kelly, R.G. Hynes, D.O. Miller, L. Weeks, J.G. Shapter, K.J. Pope, Inorg. Chem. 43 (2004) 3812.
[27] L. Zhao, L.K. Thompson, Z. Xu, D.O. Miller, D.R. Stirling, J. Chem. Soc., Dalton Trans. (2001) 1706.
[28] L.P. Battaglia, M. Carcelli, F. Ferraro, L. Mavilla, C. Pelizzi, G. Pelizzi, J. Chem. Soc., Dalton Trans. (1994) 2651.
[29] H. Ogura, S. Mineo, K. Nakagawa, S. Shiba, Yakugaka Zasshi 101 (1981) 329.
[30] J.H. Boyer, R. Borgers, L.T. Wolford, J. Am. Chem. Soc. 79 (1957) 678.
[31] V.A. Milway, L.K. Thompson, D.O. Miller, Chem. Commun. (2004) 1790.
[32] M. Julve, M. Verdaguer, A. Gleizes, M. Philoche-Levisalles, Inorg. Chem. 23 (1984) 3808.
[33] L.K. Thompson, Z. Xu, A.E. Goeta, J.A.K. Howard, H.J. Clase, D.O. Miller, Inorg. Chem. 37 (1998) 3217.
[34] E. Colacio, J.M. Domínguez-Vera, M. Ghazi, R. Kivekäs, M. Klinga, J.M. Moreno, Eur. J. Inorg. Chem. (1999) 441.
[35] E. Colacio, M. Ghazi, R. Kivekäs, J.M. Moreno, Inorg. Chem. 39 (2000) 2882.